IOPscience iopscience.iop.org

Home Search Collections Journals About Contact us My IOPscience

Switching Mode and Mechanism in Binary Oxide Resistive Random Access Memory Using Ni Electrode

This content has been downloaded from IOPscience. Please scroll down to see the full text.

2013 Jpn. J. Appl. Phys. 52 031801

(http://iopscience.iop.org/1347-4065/52/3R/031801)

View the table of contents for this issue, or go to the journal homepage for more

Download details:

IP Address: 140.113.38.11

This content was downloaded on 26/04/2014 at 07:13

Please note that terms and conditions apply.

Japanese Journal of Applied Physics 52 (2013) 031801 **REGULAR PAPER**
http://dx.doi.org/10.7567/JJAP.52.031801

Switching Mode and Mechanism in Binary Oxide Resistive Random Access Memory Using Ni Electrode

Kuan-Liang Lin[1], Tuo-Hung Hou[1*], Yao-Jen Lee[2], Jhe-Wei Chang[3], Jun-Hung Lin[3], Jiann Shieh[4], Cheng-Tung Chou[3], Tan-Fu Lei[1], Wen-Hsiung Chang[5], Wen-Yueh Jang[5], and Chen-Hsi Lin[5]

[1] *Department of Electronics Engineering and Institute of Electronics, National Chiao Tung University, Hsinchu 300, Taiwan*
[2] *National Nano Device Laboratories, Hsinchu 300, Taiwan*
[3] *Department of Chemical and Materials Engineering, National Central University, Jhongli 320, Taiwan*
[4] *Department of Materials Science and Engineering, National United University, Miaoli 360, Taiwan*
[5] *Winbond Electronics Corporation, Taichung 428, Taiwan*
E-mail: thhou@mail.nctu.edu.tw

Received July 26, 2012; accepted December 14, 2012; published online February 13, 2013

Resistive-switching (RS) modes in different CMOS-compatible binary oxides have been shown to be governed by the interplay with the Ni top electrode. Unipolar RS and metallic low-resistance state in polycrystalline HfO_2 and ZrO_2 are distinct from the preferential bipolar RS and semiconductive low-resistance state in amorphous Al_2O_3 and SiO_2. Backside secondary ion mass spectrometry (SIMS) has shown the formation of Ni filaments in HfO_2, in contrast to the formation of oxygen-vacancy filaments in Al_2O_3. The differences have been explained by strong dependence of Ni migration on the oxide crystallinity. Additionally, the RS mode can be further tailored using bilayer structures. The oxide layer next to the Si bottom electrode and its tendency of forming Ni filaments play significant roles in unipolar RS in the bilayer structures, in support of the conical-shape Ni filament model where the connecting and rupture of filaments for unipolar RS occur at the smallest diameter near the bottom electrodes. © 2013 The Japan Society of Applied Physics

1. Introduction

Resistive random access memory (RRAM) employs reversible resistive switching (RS) between low resistance state (LRS) and high resistance state (HRS) in simple metal-insulator-metal (MIM) structures for nonvolatile information storage.[1,2] In redox-based RRAM, RS has been reported to occur at local conducting filaments comprising either oxygen vacancies or metal ions in insulators. By applying appropriate SET/RESET voltage (V_{SET}/V_{RESET}) between top and bottom electrodes, the connecting and rupture of conducting filaments are triggered by three major physical mechanisms and results in different bipolar RS (BRS) and unipolar RS (URS) modes, namely electrochemical metallization of metal filaments for BRS, valance change effect of oxygen-vacancy filaments for BRS, and thermochemical effect for URS when Joule heating is predominant at RESET.[2)]

Among a wide range of materials showing RS phenomena, such as perovskite oxides, ferromagnets, chalcogenides, and binary metal oxides,[3–9] the binary metal oxides such as HfO_2 have been the most interesting because of their compatibility with advanced CMOS technology.[10,11] Furthermore, the RS modes in RRAM had been shown to depend strongly on the metal electrodes using an identical binary oxide.[12–14] In our earlier study, HfO_2 RRAM exhibited BRS with TiN/Ti, Ta and Pt top electrodes (TEs) but different URS with electrochemically active Cu and Ni TEs.[14] Among them, the HfO_2 RRAM with Ni TEs showed excellent cycling variations, endurance, retention, and low RESET current of 50 μA.[14,15] The forming and SET switching were attributed to the Ni filament formation because of the electrochemical metallization effect, i.e., Ni cations oxidized at the Ni anode migrate through HfO_2 before eventually reduced at the Si cathode. The RESET switching was attributed to the dissolution and rupture of the Ni filaments by Joule heating. However, the dependence of different binary oxides on the RS mode using an identical metal TE was less discussed. Whether or not the same type of filaments forms in different binary oxide RRAMs using the same TE requires further investigations. Therefore, the interplay between metal electrodes and binary oxides is still not completely understood.

In this study, RS modes of CMOS-compatible binary oxides including SiO_2, Al_2O_3, HfO_2, and ZrO_2 were systematically investigated using Ni TEs. Preferential BRS in amorphous Al_2O_3 and SiO_2 and URS in polycrystalline HfO_2 and ZrO_2 suggest a RS mechanism depending strongly on the binary oxide films. Backside secondary ion mass spectrometry (SIMS) confirmed substantial Ni migration in the polycrystalline HfO_2 but not in the amorphous Al_2O_3 after forming, supporting that the formation of Ni conducting filaments was responsible for the observed URS. The URS location where the connecting and rupture of conducting filaments take place at V_{SET} and V_{RESET} was further examined using various bilayer structures. The oxide layer next to the bottom electrode (BE) was found to play a significant role in URS. The result was in good agreement with the conical-shape Ni filament model,[15,16] where the URS location was postulated to be near the BE with a smaller filament diameter.

2. Experimental Procedure

CMOS-compatible Ni/binary oxide/Si memory cells using SiO_2, Al_2O_3, HfO_2, and ZrO_2 as monolayer or bilayer RS structures were fabricated on heavily doped p^+-Si substrates. After standard RCA clean and rapid thermal oxidation at 500 °C for 10 s in ambient O_2, four different 10-nm monolayer films, HfO_2/SiO_2 (10 nm/2–5 nm), HfO_2/Al_2O_3 (10 nm/2–5 nm), and Al_2O_3/HfO_2 (2–15 nm/10 nm) bilayer films were deposited. SiO_2 was deposited by low-pressure chemical vapor deposition at 680 °C using $Si(OC_2H_5)_4$ (TEOS) as the precursor. HfO_2 and Al_2O_3 were deposited by metal organic chemical vapor deposition at 500 °C using $Hf(OtBu)_2(mmp)_2/O_2$ and $Al[OCH(CH_3)_2]_3/O_2$ as the precursors, respectively. ZrO_2 was deposited by atomic

 © 2013 The Japan Society of Applied Physics

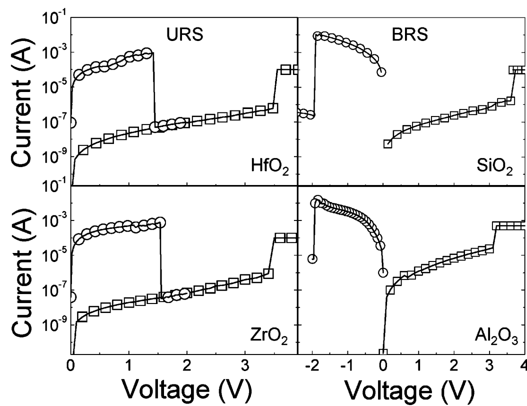

Fig. 1. Typical RS *I–V* characteristics of 10-nm HfO_2, ZrO_2, SiO_2, and Al_2O_3 with Ni TEs.

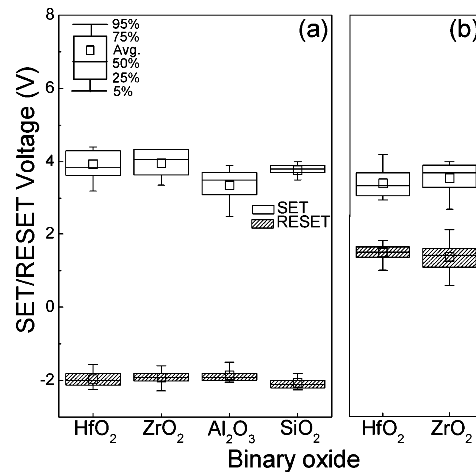

Fig. 2. Statistical distribution of switching voltages of (a) BRS in HfO_2, ZrO_2, Al_2O_3, and SiO_2 devices, and (b) URS in HfO_2 and ZrO_2 devices. At least 30 switching cycles were measured for each device type.

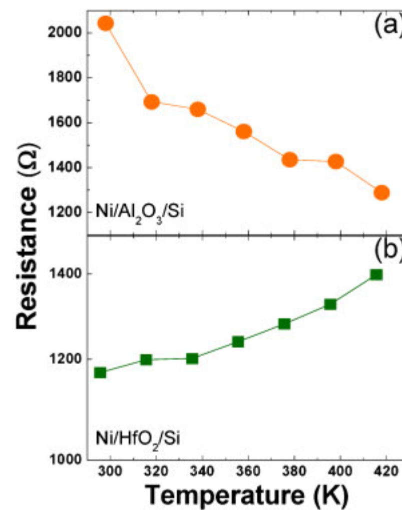

Fig. 3. (Color online) Temperature dependence of the LRS resistance for the (a) $Ni/Al_2O_3/Si$ and (b) $Ni/HfO_2/Si$ devices. Negative and positive temperature coefficients of LRS were found in the Al_2O_3 and HfO_2 devices, respectively.

layer deposition at 300 °C using $Zr[N(CH_3)(C_2H_5)]_4$ (TEMAZr) and O_3 as the precursors, followed by post annealing at 400 °C. Finally, Ni TEs with a thickness of 100 nm and a diameter of 200 µm were deposited by DC sputtering and a shadow mask process. All devices were measured using an Agilent 4156B semiconductor parameter analyzer by applying voltage to the top electrodes while the p^+-silicon substrates were grounded.

3. Results and Discussion

Figure 1 illustrates the typical RS current–voltage (*I–V*) characteristics of the four binary oxides with Ni TEs using DC voltage sweep. To initialize RS, a positive-polarity forming process (not shown) was necessary using a fixed current compliance of 100 µA. In Fig. 1, the HfO_2 and ZrO_2 devices showed URS with positive V_{SET} and V_{RESET}, whereas those with SiO_2 and Al_2O_3 exhibited only BRS. The HfO_2 and ZrO_2 devices can also be reset at negative V_{RESET} for BRS. The RS properties reported here were reproducible with at least several dozen cycles of continuous voltage sweeps. Figure 2 shows the statistical distributions of V_{SET} and V_{RESET} of different binary oxides, where both BRS and URS existed in the HfO_2 and ZrO_2 devices. The lack of URS in the SiO_2 and Al_2O_3 devices was significantly different from the coexistence of URS and BRS in the HfO_2 and ZrO_2 devices. Furthermore, the temperature-dependent LRS resistances of the $Ni/Al_2O_3/Si$ and $Ni/HfO_2/Si$ devices were measured, as shown in Figs. 3(a) and 3(b). Negative temperature coefficient of LRS in the $Ni/Al_2O_3/Si$ device suggested a transport mechanism related to the charge hopping through semiconductive filaments. By contrast, positive temperature coefficient of LRS in the $Ni/HfO_2/Si$ device exhibited typical metallic characteristics. The results implied that different compositions of conductive filaments might exist in the $Ni/Al_2O_3/Si$ and $Ni/HfO_2/Si$ devices and result in the different RS modes.

In our earlier study of the HfO_2-based RRAM with various TEs,[14] 50-nm HfO_2 with TiN/Ti, Ta, and Pt TEs also showed preferential BRS. Oxygen-deficient filaments in HfO_2 were confirmed by local energy dispersive X-ray spectroscopy (EDX)[14] and believed to be responsible for BRS. Therefore, the BRS in $Ni/Al_2O_3/Si$ and $Ni/SiO_2/Si$ might also correlate to oxygen vacancy-related filaments in the bulk of binary oxides. This is further supported by the fact that the similar preferential BRS in Al_2O_3 and SiO_2 was also observed using an inert Pt TE in Fig. 4, where filament compositions other than oxygen vacancy were less likely. Alternatively, the URS in $Ni/HfO_2/Si$ had been attributed to the formation of metallic Ni filaments, confirmed by excessive Ni diffusion by SIMS and high-resolution transmission electron microscopy (HRTEM) from several research groups.[11,14,17] The resembling RS characteristics of $Ni/ZrO_2/Si$ suggested a similar mechanism.

Figure 5 compares the backside SIMS profiles of the $Ni/Al_2O_3/Si$ and $Ni/HfO_2/Si$ devices before and after positive forming. Backside SIMS profiling suppressed the artificial Ni knock-on effect from the Ni TEs in the conventional front-side SIMS, and allowed the investigation of the Ni filament formation in RRAMs.[14] Some intermixing at the Ni/HfO_2 and Ni/Al_2O_3 interfaces was attributed to the

 © 2013 The Japan Society of Applied Physics

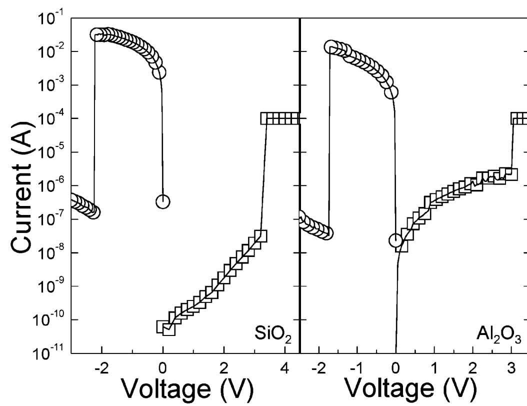

Fig. 4. Typical BRS characteristics in SiO_2 and Al_2O_3 devices with Pt TEs.

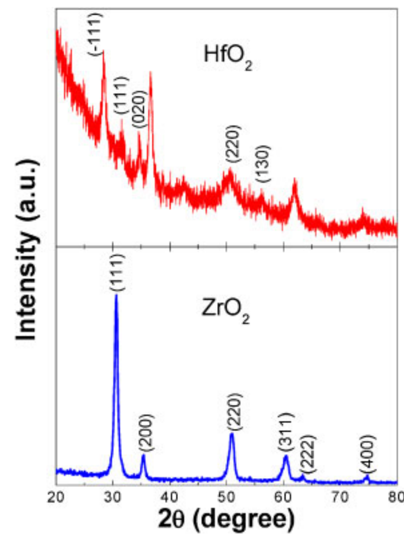

Fig. 6. (Color online) XRD patterns of HfO_2 and ZrO_2 thin films deposited on the p^+-Si substrates. Both HfO_2 and ZrO_2 films were polycrystalline.

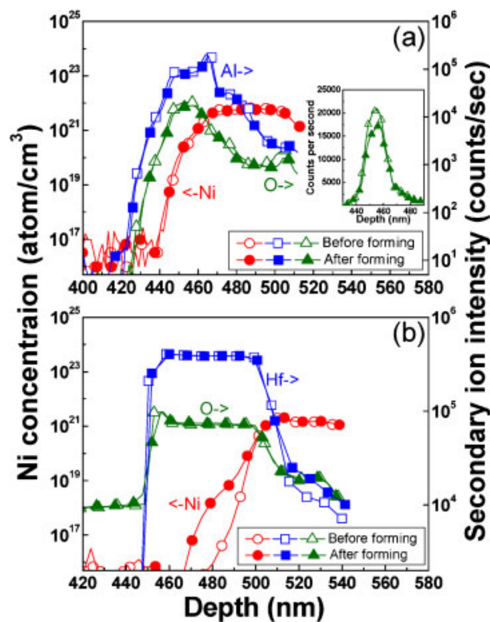

Fig. 5. (Color online) (a) Backside SIMS profiling of the $Ni/Al_2O_3/Si$ device before and after positive forming. The profiling direction was from Si into Al_2O_3. Inset illustrates the oxygen profile in Al_2O_3 in linear scale, showing decreasing oxygen intensity after forming. (b) The previous analysis on a Ni/50-nm HfO_2/Si device[14] using identical processes as this study is also replotted for easy comparison. Substantial Ni elements migrated into HfO_2 after forming whereas the Ni profile of the $Ni/Al_2O_3/Si$ device remained unchanged.

Table I. Summary of RS modes of different binary oxide RRAMs in Ref. 14 and this study.

	TE	Binary oxide	BE	BRS	URS	Note
1	TiN/Ti	HfO_2	Si	●		Ref. 14
2	Ta	HfO_2	Si	●		Ref. 14
3	Pt	HfO_2	Si	●		Ref. 14
4	Cu	HfO_2	Si	●	●	Ref. 14
5	Ni	HfO_2	Si	●	●	
6	Ni	ZrO_2	Si	●	●	
7	Ni	SiO_2	Si	●		
8	Ni	Al_2O_3	Si	●		
9	Pt	SiO_2	Si	●		
10	Pt	Al_2O_3	Si	●		

sputtering process of the Ni deposition. While substantial Ni migrated from the TE into the HfO_2 layer after forming with the amount decreased gradually toward the Si BE, the Ni migration into the Al_2O_3 layer after forming was prohibited and the peak oxygen intensity in Al_2O_3 was reduced by 20% to become more oxygen deficient. Therefore, Ni filaments were believed to be formed only in HfO_2 but not in Al_2O_3 and responsible for the distinct difference in the RS mode and the temperature coefficient of LRS. The HfO_2 and ZrO_2 films used in this study were polycrystalline according to X-ray diffraction (XRD) analysis, as shown in Fig. 6. The oriented grain boundaries were suspected to allow rapid Ni migration across HfO_2 and ZrO_2. By contrast, the amorphous SiO_2 and Al_2O_3 lack of oriented grain boundaries likely suppressed Ni migration. Note that amorphous Al_2O_3 had been explored as an excellent diffusion barrier for Cu/low-κ interconnects[18] and the crystallinity is generally believed to have profound impacts on the effectiveness of Cu diffusion barriers.[19]

Table I summarizes the interplay between TE and binary oxide materials and the corresponding RS modes in this work and in Ref. 14. According to the aforementioned physical and electrical evidence, we summarize the plausible RS mechanisms as follows: The preferential BRS may be attributed to the formation of oxygen-deficient filaments. The connecting and rupture were driven by the migration of oxygen anions using bipolar electric field. URS existed only when using electrochemically active metals of Ni and Cu as anode electrodes, accompanied by polycrystalline binary oxides of HfO_2 and ZrO_2. Because the binary oxides acted as solid electrolytes in an electrochemical cell,[5] different crystallinities of binary oxides significantly affected the cation migration and thus the formation of metallic filaments. The URS RESET was enabled because of Joule heating and thermal dissolution of the Ni filaments.

 © 2013 The Japan Society of Applied Physics

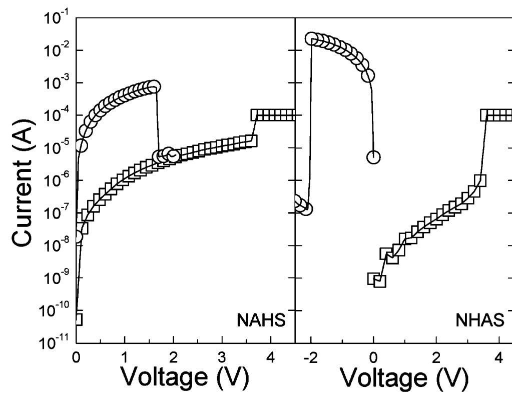

Fig. 7. Typical URS characteristics in the Ni/3-nm Al_2O_3/10-nm HfO_2/Si (NAHS) device and typical BRS characteristics in the Ni/10-nm HfO_2/3-nm Al_2O_3/Si (NHAS) device.

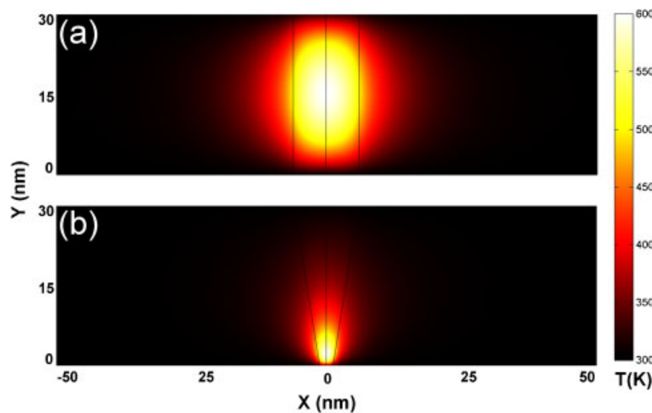

Fig. 8. (Color online) Temperature profile simulation at RESET in (a) a cylindrical and (b) a conical-shape filament. Joule heating is enhanced near the bottom electrode with a smaller diameter in the conical-shaped filament because of the current-crowding effect. The RESET condition was defined when the maximum temperature reached 600 K.

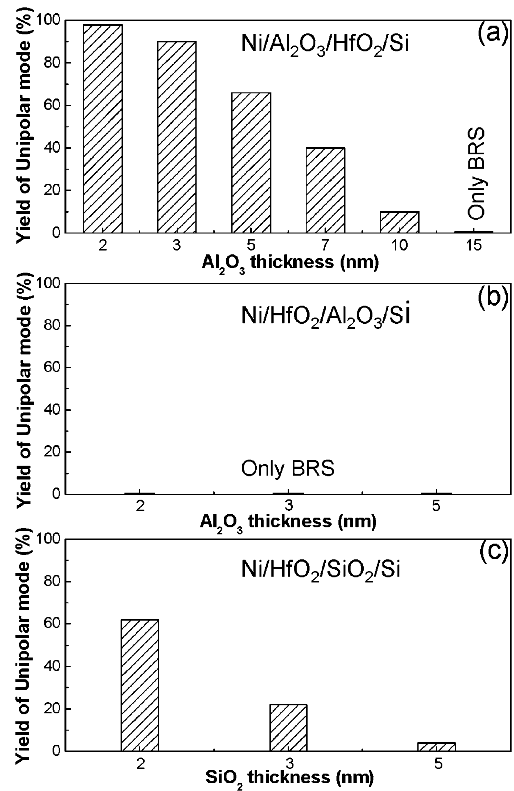

Fig. 9. Device yield of unipolar RS in (a) $Ni/Al_2O_3/HfO_2/Si$, (b) $Ni/HfO_2/Al_2O_3/Si$, and (c) $Ni/HfO_2/SiO_2/Si$ structures with various Al_2O_3 and SiO_2 thickness. The thickness of HfO_2 for all samples was 10 nm. The yield device was defined allowing at least five consecutive unipolar RS cycles, and total 50 devices were measured for each structure.

The design of binary oxide bilayer structures can facilitate in-depth understanding on the URS location where the connecting and rupture of conducting filaments take place at V_{SET} and V_{RESET}. The Ni/3-nm Al_2O_3/10-nm HfO_2/Si (NAHS) and Ni/10-nm HfO_2/3-nm Al_2O_3/Si (NHAS) devices were fabricated using an identical process except the reversed deposition sequence of HfO_2 and Al_2O_3. Both devices required a similar forming voltage of approximately 7.5 V. URS was observed in the NAHS device in contrast to preferential BRS in the NHAS device, as shown in Fig. 7. Because of the preferential BRS in Al_2O_3 and the coexistence of BRS and URS in HfO_2, the RS mode in the bilayer devices is postulated to be governed by the binary oxide layer immediately next to the BE.

It was reported that the filament morphology of the $Ni/HfO_2/Si$ URS devices may be consistently explained by a conical-shape filament model, where the connecting and rupture of Ni filaments occurred locally near the BE with a smaller diameter.[15] The numerical simulation of the temperature profile at RESET in a cylindrical and a conical-shape filament are shown in Fig. 8. The RESET temperature of 600 K was chosen for illustration purpose only, but agreed with the fact that the Ni filaments may be ruptured above 573 K.[14] The temperature rise because of Joule heating was the highest at the middle of the cylindrical filament but near the BE of the conical-shape filament. Therefore, the tendency of Ni filament formation in the oxide layer next to the BE played a significant role in URS.

The thickness effect of Al_2O_3 in the NAHS and NHAS bilayer structures was also examined. Another Ni/10-nm $HfO_2/SiO_2/Si$ (NHSS) bilayer structure with various SiO_2 thicknesses was also fabricated for comparison. All structures demonstrated high-yield BRS. Additionally, Fig. 9 shows the device yield of URS in all bilayer structures. The yield device was defined allowing at least five consecutive URS cycles, and total 50 devices were measured for each structure. For the NAHS structures, the yield for URS degraded as the Al_2O_3 thickness increased. This may be explained by suppressing Ni migration into HfO_2 because of the increasing thickness of the Al_2O_3 diffusion barrier between the Ni TE and HfO_2. On the other hand, all NHAS devices exhibited only BRS regardless of the Al_2O_3 thickness investigated in this study. In contrast to the NAHS structures where abundant Ni was supplied from the TE, Ni migration was filtered first by HfO_2 before much less amount of Ni can reach the BE. The result suggests that a very thin Al_2O_3 layer on top of the BE was sufficient to prevent the formation of complete Ni filaments. By contrast, reproducible URS was observed in the NHSS devices with thinner SiO_2 layers whereas the yield of URS degraded to nearly zero with a SiO_2 layer of 5 nm. SiO_2 is known to be an inferior diffusion barrier as compared with Al_2O_3,[18] and

 © 2013 The Japan Society of Applied Physics

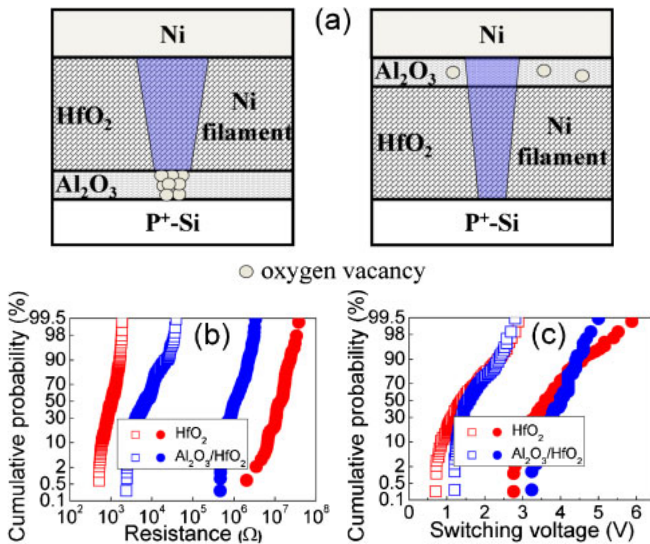

Fig. 10. (Color online) (a) Schematic of different composition of conducting filaments in $Ni/HfO_2/Al_2O_3/Si$ and $Ni/Al_2O_3/HfO_2/Si$ devices at LRS. Cumulative probability of (b) R_{HRS} and R_{LRS} and (c) V_{SET} and V_{RESET} for $Ni/HfO_2/Si$ and Ni/3-nm $Al_2O_3/HfO_2/Si$ devices under URS.

thin SiO_2 might allow the formation of Ni filaments and URS. The strong dependence of the SiO_2 thickness between the Si BE and HfO_2 also explains stable URS in $Ni/HfO_2/Si$, where a thin interfacial layer of SiO_x (about 1.5 nm) existed between HfO_2 and Si,[14] whereas only BRS existed in the aforementioned 10-nm SiO_2 monolayer.

Figure 10(a) depicts a RS model where the composition of the filament in bilayer structures depends on the metal cation diffusivity in binary oxides. For the NHAS device, Ni ions diffuse into polycrystalline HfO_2 through grain boundaries before eventually blocked by the amorphous Al_2O_3 barrier during the forming and SET process. Hence, the dominant composition of conducting filaments was Ni in HfO_2 and oxygen vacancy in Al_2O_3. The preferential bipolar RESET was consistent with that in $Ni/Al_2O_3/Si$ and may be attributed to the rupture of the oxygen-vacancy filaments in Al_2O_3. However, further investigations would be necessary to exclude the possibility of rupturing the Ni filaments in HfO_2 under bipolar RESET driven by electric field. For the NAHS device with a thinner Al_2O_3 layer, sufficient Ni ions were able to diffuse through thin Al_2O_3 into HfO_2 because of the abundant source, and formed conical-shape Ni filaments necessary for URS. However, the filament size regulated by the top Al_2O_3 layer is expected to be smaller in the NAHS device as compared with that in the $Ni/HfO_2/Si$ monolayer device. This is further supported by the tighter distribution of HRS resistance (R_{HRS}), LRS resistance (R_{LRS}), V_{SET}, and V_{RESET} of the NAHS bilayer device, as shown in Figs. 10(b) and 10(c). The higher R_{LRS} and lower R_{HRS} are the signature of the reduced filament size because of the increase of filament resistance at LRS and residual small filaments at HRS that were unable to be completely ruptured because of insufficient RESET power.[15]

4. Conclusions

The RS modes of binary oxides, including SiO_2, HfO_2, Al_2O_3, and ZrO_2, were investigated using Ni TEs. URS in HfO_2 and ZrO_2 correlated with metallic Ni filaments, whereas preferential BRS in Al_2O_3 and SiO_2 correlated with oxygen-deficient filaments. The composition difference of the conducting filaments was confirmed by the backside SIMS analysis, showing the suppression of Ni migration in amorphous Al_2O_3 as compared to that in polycrystalline HfO_2. Furthermore, the RS mode can be further tailored using bilayer structures. The NHAS bilayer structure displayed BRS only, but the NAHS bilayer with thinner Al_2O_3 was capable of URS. The absence of URS in the NHAS structure implies that the filament connecting and rupture occurred locally near the Si BE for URS, in support of the conical-shape Ni filament model. Additionally, the thickness effect of the Al_2O_3 and SiO_2 interfacial layers in the bilayer structures can be consistently explained by the Ni migration. The results suggest new possibilities of designing the RS mode using engineered interfacial layers between binary oxides and metal electrodes.

Acknowledgments

The experimental work was performed at the Nano Facility Center (NFC) of National Chiao-Tung University and National Nano Device Laboratories (NDL). Financial support was partially provided by National Science Council of the Republic of China under contract No. NSC 97-2218-E-009-039-MY3.

1) I. G. Baek, M. S. Lee, S. Seo, M. J. Lee, D. H. Seo, D. S. Suh, J. C. Park, S. O. Park, H. S. Kim, I. K. Yoo, U.-I. Chung, and J. T. Moon: IEDM Tech. Dig., 2004, p. 587.
2) R. Waser, R. Dittmann, G. Staikov, and K. Szot: Adv. Mater. **21** (2009) 2632.
3) C. C. Lin, C. Y. Lin, M. H. Lin, C. H. Lin, and T. Y. Tseng: Appl. Phys. Lett. **93** (2008) 042115.
4) D. Hsu, J. G. Lin, and W. F. Wu: Appl. Phys. Lett. **88** (2006) 222507.
5) M. N. Kozicki, M. Park, and M. Mitkova: IEEE Trans. Nanotechnol. **4** (2005) 331.
6) S. Seo, M. J. Lee, D. H. Seo, E. J. Jeoung, D.-S. Suh, Y. S. Joung, I. K. Yoo, I. R. Hwang, S. H. Kim, I. S. Byun, J.-S. Kim, J. S. Choi, and B. H. Park: Appl. Phys. Lett. **85** (2004) 5655.
7) W. Guan, S. Long, Q. Liu, M. Liu, and W. Wang: IEEE Electron Device Lett. **29** (2008) 434.
8) W. Y. Chang, C. A. Lin, J. H. He, and T. B. Wu: Appl. Phys. Lett. **96** (2010) 242109.
9) T. M. Pan and C. H. Lu: Appl. Phys. Lett. **99** (2011) 113509.
10) Y. S. Chen, H. Y. Lee, P. S. Chen, P. Y. Gu, C. W. Chen, W. P. Lin, W. H. Liu, Y. Y. Hsu, S. S. Sheu, P. C. Chiang, W. S. Chen, F. T. Chen, C. H. Lien, and M.-J. Tsai: IEDM Tech. Dig., 2009, p. 105.
11) X. Li, W. H. Liu, N. Raghavan, M. Bosman, and K. L. Pey: Appl. Phys. Lett. **97** (2010) 202904.
12) C. Y. Lin, C. Y. Wu, C. Y. Wu, T. C. Lee, F. L. Yang, C. Hu, and T. Y. Tseng: IEEE Electron Device Lett. **28** (2007) 366.
13) C. B. Lee, B. S. Kang, A. Benayad, M. J. Lee, S. E. Ahn, K. H. Kim, G. Stefanovich, Y. Park, and I. K. Yoo: Appl. Phys. Lett. **93** (2008) 042115.
14) K. L. Lin, T. H. Hou, J. Shieh, J. H. Lin, C. T. Chou, and Y. J. Lee: J. Appl. Phys. **109** (2011) 084104.
15) T. H. Hou, K. L. Lin, J. Shieh, J. H. Lin, C. T. Chou, and Y. J. Lee: Appl. Phys. Lett. **98** (2011) 103511.
16) K. M. Kim and C. S. Hwang: Appl. Phys. Lett. **94** (2009) 122109.
17) Y. Y. Chen, G. Pourtois, C. Adelmann, L. Goux, B. Govoreanu, R. Degreave, M. Jurczak, J. A. Kittl, G. Groeseneken, and D. J. Wouters: Appl. Phys. Lett. **100** (2012) 113513.
18) D. C. Perng, J. B. Yeh, K. C. Hsu, and S. W. Tsai: Thin Solid Films **518** (2010) 1648.
19) Z. H. Cao, K. Hu, and X. K. Meng: J. Appl. Phys. **106** (2009) 113513.

 © 2013 The Japan Society of Applied Physics